Chemistry in embedded disks: setting the stage for planet formation

Hoff, M.L.R. van 't

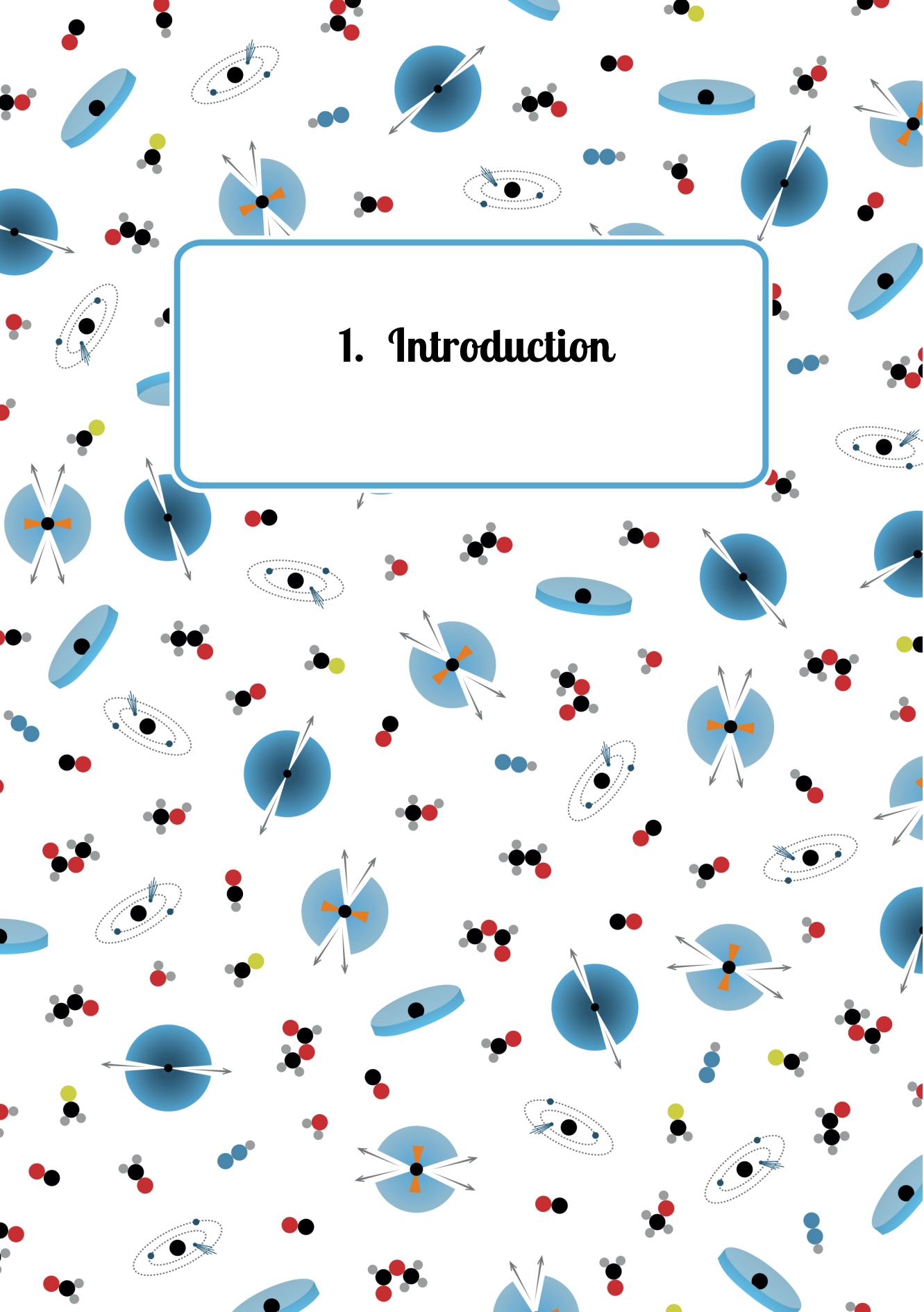

1. Introduction

For centuries, people have gazed at the stars and planets, and wondered about our place in the cosmos. Where do we come from? And, are we alone? With the discovery of more than 3000 planets around other stars in the last few decades[1], the potential of life in other solar systems has become reality. These planetary systems display a large diversity in size, and the number and types of planets, but our own Solar System seems atypical (see e.g., Raymond et al. 2019), immediately raising the question whether the occurence of life is uncommon as well. One way to try and answer these questions is by examining the properties of the discovered planets, for example, their atmospheric composition, and comparing that to what we think are the requirements for life. Another way is to study the material around newborn stars that will eventually make up planets. On the one hand, comparing the composition of planetary building blocks to the composition of Solar System comets, which are remnants of the young Solar System, can tell whether the initial conditions for the formation of the Solar System are unique or very common. On the other hand, using this information in planet formation models can predict the likelihood of forming an Earth-like planet under given conditions. Moreover, studying the chemical complexity at these early stages can tell us whether the building blocks for life are formed in space, and possibly delivered to young planets by cometary bodies, or whether life has to start from very simple molecules on a planetary surface.

This thesis utilizes the approach of studying the planet-forming material and focuses on the initial stage of planet formation, the so-called "embedded stage", in which the planetary building blocks start to form in a disk around the young protostar that is still embedded in its natal cloud. The advent of the Atacama Large Millimeter/submillimeter Array (ALMA) in 2011 has allowed the study of these objects at planetary-system scales, and this thesis uses observations of different molecular species to characterize the physical and chemical conditions at the onset of planet formation.

1.1 Formation of low-mass stars and planetary systems

Star formation occurs in dense ($n \sim 10^4 - 10^5$ cm^{-3}) and cold ($T \sim 10 - 20$ K) regions of giant molecular clouds. After the formation of a prestellar core, the early evolution of low mass stars ($M \lesssim 2\ M_\odot$) can be divided into four evolutionary *Stages* (Fig. 1.1; Shu et al. 1987). Observationally, the different phases are categorized into *Classes*, as will be described in Sect. 1.4.1. The gravitational collapse of the prestellar core results in a protostar surrounded by an infalling envelope. In this initial stage (*Stage 0*), the envelope mass is much larger than the central protostellar mass. Due to accretion, the protostellar mass increases and exceeds the envelope mass after $\sim 10^5$ years (*Stage I*). In addition, a disk begins to form during Stage 0 to conserve the angular momentum of the rotating infalling material. Stage 0 and I are referred to as the *protostellar* or *embedded stage*. The envelope dissipates due to accretion onto the disk and mass loss via bipolar outflows such that after $\sim 10^{5-6}$ years, a gas-rich protoplanetary disk is left surrounding a pre-main sequence star (*Stage II*). Accretion finally ceases (after $\sim 10^{6-7}$ years) as disk material grows into planets and dissipates due to processes like photoevaporation. In *Stage III*, the pre-main sequence star is surrounded by a gas-poor disk consisting mainly of dust created by collisions of larger bodies. Finally, the star reaches the main sequence and a planetary system is born. A more detailed description is given in the following sections.

[1] see `http://exoplanets.org` and `http://exoplanet.eu`

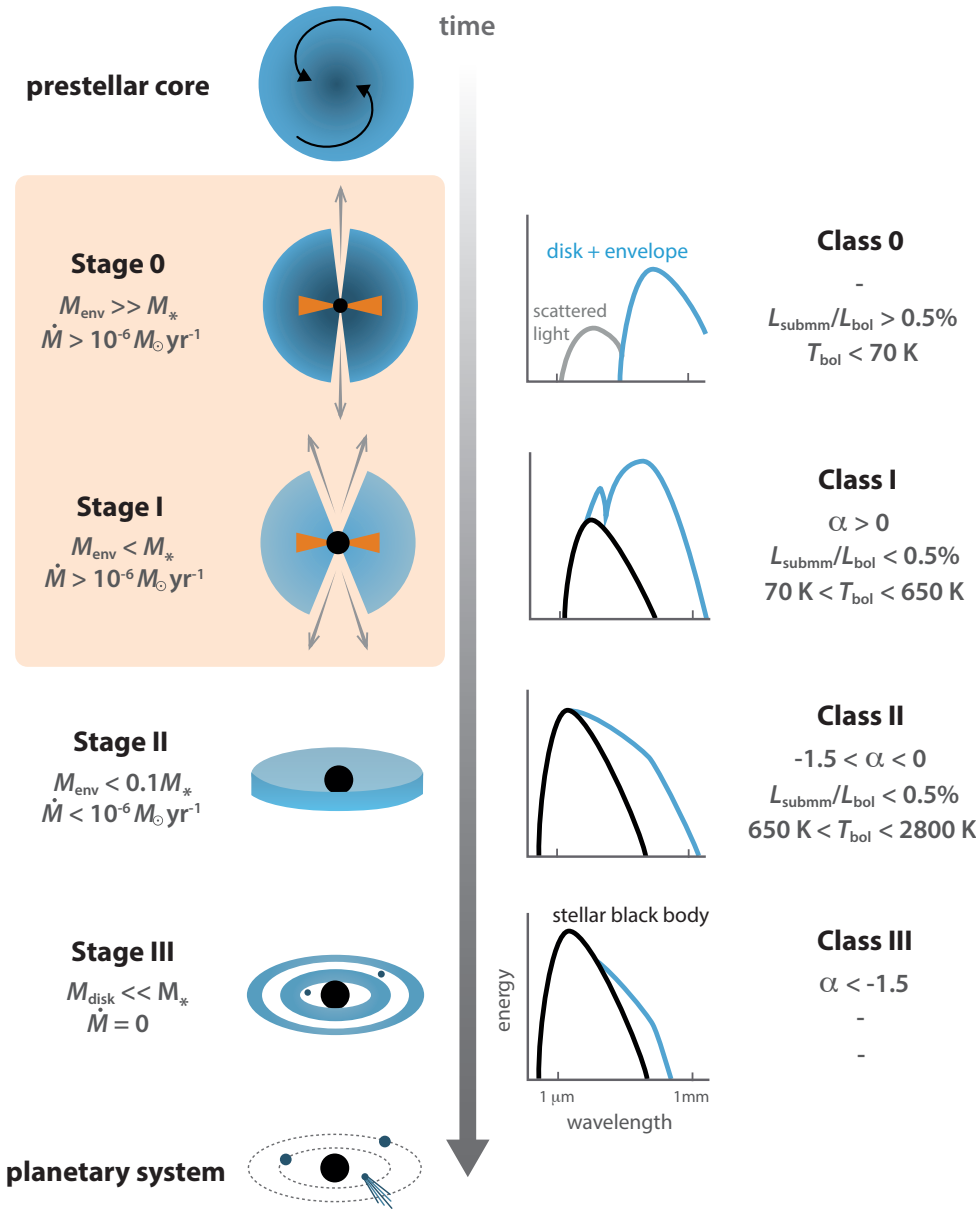

Figure 1.1: Schematic overview of the different stages of low-mass star formation (*left panels*) and the observational classification based on the spectral energy distribution (SED; *right panels*). The embedded phase that is the focus of this thesis is marked by the orange box. Stage II disks are also referred to as protoplanetary disks.

1.1.1 Protostar formation

The material in giant molecular clouds (∼10–100 pc) is not uniformly distributed, but rather concentrated in filamentary structures with typical widths of ∼0.1 pc (André et al. 2010; Kennicutt & Evans 2012). These filaments fragment into smaller fibers that in turn are the parent structures from which dense cores form (e.g., Hacar & Tafalla 2011). The exact formation mechanism for these cores is still debated, with many scenarios suggested between two extreme paradigms: quasi-static contraction mediated by ambipolar-diffusion and gravo-turbulent fragmentation driven by supersonic motions (see e.g., reviews by Ward-Thompson et al. 2007; André et al. 2014).

The collapse of such a *prestellar core* results in a first hydrostatic core (FHSC) once the inner region becomes opaque to radiation (Larson 1969). The FHSC is a short lived phase (0.5–50 kyr) with a low luminosity ($< 0.1\ L_\odot$), low mass (0.01–0.1 $M_\odot$) central object (e.g., Boss & Yorke 1995; Tomida et al. 2010). Several candidate FHSC have been proposed, but none have been unambigously identified. As the FHSC continues to accrete mass, the central temperature increases until temperatures of ∼2000 K are reached. Now H_2 starts to dissociate which prevents the temperature from rising and balancing gravity. This leads to a second collapse, forming a protostar deeply embedded in an envelope of infalling material (Larson 1969). Highly collimated bipolar outflows are typically observed during this early phase and aid in mass loss and angular momentum conservation (see e.g., reviews by Frank et al. 2014; Bally 2016).

1.1.2 Disk formation

The formation of a circumstellar disk is a natural consequence of angular momentum conservation during the collapse of a rotating core (Cassen & Moosman 1981; Terebey et al. 1984), and hydrodynamical simulations readily form large (>100 AU) and massive disks early in the embedded phase (e.g., Yorke et al. 1993). Initial observations suggest that, in principle, cores have enough angular momentum to form 100 AU-sized rotationally supported disks (e.g., Goodman et al. 1993; Caselli et al. 2002a), but with higher angular resolution and higher sensitivity observations, organized rotation of cores is found less frequently (e.g., Tobin et al. 2012a). Instead, angular momentum may be the result of residual small-scale turbulent motions or gravitational torques between cloud overdensities (Offner et al. 2016; Kuznetsova et al. 2019).

However, disk formation is far more subtle in the presence of magnetic fields (see e.g., reviews by Li et al. 2014; Lizano & Galli 2015). Ideal magnetohydrodynamic (MHD) simulations show that magnetic braking prevents the formation of a rotationally supported disk: as the material collapses, the magnetic field is dragged inward as well, increasing the field strength toward smaller radii such that the infalling material becomes dominated by the magnetic field in the inner region. Because the magnetic field remains connected to the slower rotating outer part of the envelope, all angular momentum can be removed from the collapsing inner envelope. Instead of a rotationally supported disk, a non-equilibruim flattened structure (a pseudo-disk) is formed, as predicted by Galli & Shu (1993a,b). This "magnetic braking catastrophe" has been confirmed analytically and in multiple numerical simulations (e.g., Galli et al. 2006; Mellon & Li 2008).

Since protoplanetary disks are ubiquitiously observed (e.g., Ansdell et al. 2016), several potential solutions are being investigated and remain an active topic of investigation (see e.g., review by Li et al. 2014). Since dense cores are only slightly ionized

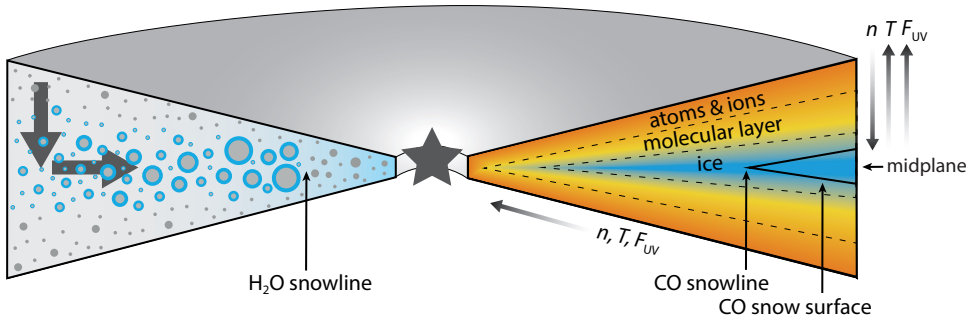

Figure 1.2: Physical and chemical structure of a protoplanetary disk. The *left side* shows the growth of ice covered dust grains as they settle toward the midplane and drift inward. Inside the water snowline all ice has evaporated and these bare grains are more prone to fragmentation. The *right side* shows the layered chemical structure due to vertical and radial gradients in density (n), temperature (T) and UV flux ($F_{\rm UV}$).

(with a typical electron fractional abundance of $\sim 10^{-7}$; Bergin & Tafalla 2007), the magnetic field is not expected to be perfectly frozen into the material (as is assumed in the ideal MHD case). Multiple groups have therefore developed numerical simulations to study non-ideal MHD effects (ambipolar diffusion, Ohmic dissipation, and the Hall effect). Although the exact conditions for disk formation remain widely debated, the general conclusion so far seems to be that small (10–100 AU) rotationally supported disks can form in the early stage of protostar formation (see e.g., Tsukamoto et al. 2017 and Wurster et al. 2018 for recent results). Other effects that can promote disk formation are misalignment between the magnetic field and the rotation axis, turbulence and rapid depletion of the envelope. A handful of rotationally supported disks has now indeed been observed around deeply embedded objects (see Sect. 1.4).

Once a disk is formed, most mass is likely accreted onto the protostar through the disk. Two main processes have been proposed for the transport of mass and angular momentum in disks (see e.g., the review by Turner et al. 2014): viscous torques due to turbulence triggered by the magneto-rotational instability (MRI; Balbus & Hawley 1991) and gravitational torques induced by gravitational instability (GI; Lin & Pringle 1987; Laughlin & Bodenheimer 1994). However, simpler numerical models based on the Shakura & Sunyaev (1973) α-parametrization are often used because they circumvent the complicated physics of MRI and GI by treating both processes as a local viscous transport mechanism. In these models the strength of the turbulent viscosity is described with a dimensionless parameter α. Angular momentum can also be removed through winds, either launched close to the protostar (X-winds) or from the disk surface (disk winds).

1.1.3 Planet formation

Planets form from the dust and gas in disks (for recent reviews, see e.g., Johansen & Lambrechts 2017; Izidoro & Raymond 2018), and the first step in this formation process is the growth of micrometer-sized dust grains into millimeter and centimeter-sized particles (see e.g., the review by Testi et al. 2014). Both laboratory experiments and numerical simulations show that coagulation into mm and cm-sized particles (*pebbles*) occurs quite easily through collisions (e.g., Blum & Wurm 2008). However, further growth faces several obstacles and is the topic of active research. If particles grow be-

yond cm size, their relative velocities become so large that they fragment or bounce, instead of stick, upon impact. These barriers are known as the "bouncing" and "fragmentation barrier", respectively. Even if particles could grow efficiently, the formation of km-sized bodies is hampered by the "drift barrier": because the gas orbits at slightly sub-Keplerian speed due to a pressure gradient, larger particles on a Keplerian orbit feel a headwind that creates a drag force (Whipple 1972; Weidenschilling 1977). The subsequent loss of angular momentum then causes them to drift inward (**Fig. 1.2**). This radial drift is important for mm and cm-sized grains, but is especially efficient for decimeter to meter-sized particles; a meter-sized object at 1 AU falls toward the star in ∼100 years.

A way to overcome the drift barrier is by trapping particles in localized regions of increased pressure, so-called "pressure bumps". Many mechanisms have been put forward to create pressure bumps and trap particles (see e.g., Pinilla et al. 2017 for a review), such as vortices, spiral arms in self-gravitating disks, magneto-rotational instability and snowlines. In addition, particles can be trapped at the inner edge of the "dead zone" (the region in the disk where the ionisation degree is too low for coupling of the gas to the magnetic field) and at the outer edge of the gap carved by a Jupiter-mass planet. Inside pressure bumps, particles may grow into kilometer-sized bodies (*planetesimals*), because there is more time to grow and the collisional speeds are lower and thus more amenable to growth. If the particle density becomes high enough planetesimals can form by gravitational collapse of cm-sized pebbles.

Friction with the gas may also result in particle concentration by a mechanism called the "streaming instability" if an initial enhancement of solids is present (Youdin & Goodman 2005; Johansen et al. 2007). The region just outside the water snowline seems to be a favorable place to trigger the streaming instability (e.g., Schoonenberg & Ormel 2017; Drążkowska & Alibert 2017), because the solid density will be enhanced by freeze-out of gaseous water that diffuses outward across the snowline (Stevenson & Lunine 1988). Planetesimal formation may also be enhanced outside the water snowline because icy particles are more sticky than silicate grains (e.g., Wada et al. 2011) and can thus grow to larger sizes before they fragment or even grow to highly porous aggregates that can overcome the drift barrier (Okuzumi et al. 2012).

Once km-sized planetesimals have formed, subsequent growth is dominated by gravity. Currently, two main theories exist for planetesimal growth: growth by collisions between planetesimals ("planetesimal accretion"; Kokubo & Ida e.g., 1996; Tanaka & Ida e.g., 1999) and accretion of the remaining cm-sized pebbles ("pebble accretion", Ormel & Klahr 2010; Lambrechts & Johansen 2012). In the traditional planetesimal accretion scheme, planetary embryos emerge through a phase of runaway growth in which the largest bodies grow the fastest. In order to form a giant planet, a sufficiently large core ($\sim$10 $M_{\rm Earth}$) must form in order to start gas accretion (e.g., Pollack et al. 1996). However, it is very hard to form such cores within the disk lifetime through planetesimal accretion, especially at the distance of Uranus and Neptune (e.g., Thommes et al. 2003). In contrast, growth through the accretion of pebbles can be orders of magnitude faster and thus solve this issue once there are planetesimals to accrete on. Another proposed solution for giant planets at large orbits is formation through gravitational instability (GI) in the gas (Boss 1997; Boley 2009), a scenario most likely to happen in the outer regions of massive ($M_{\rm disk} \gtrsim 0.1 M_*$) or cold disks ($T \lesssim$ 30-40 K). However, GI is more likely to form companion stars than planets (e.g., Kratter et al. 2010).

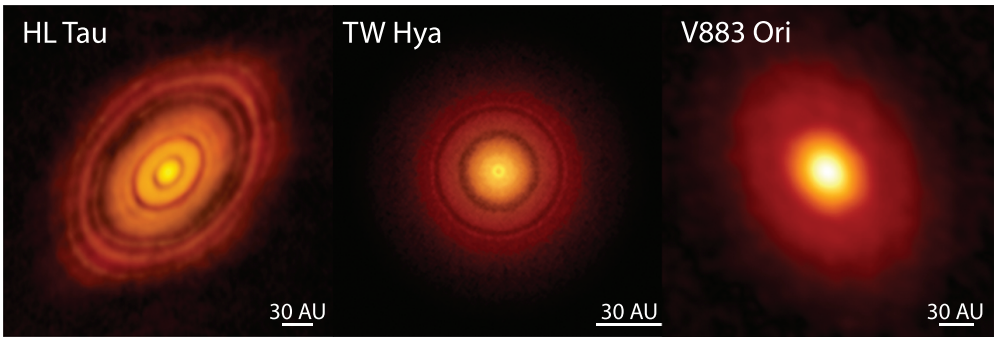

Figure 1.3: Rings are ubiquitously observed in ALMA continuum images of disks. If they are caused by forming planets (which is still highly debated), planet formation has to start in the embedded phase, because HL Tau (*left panel*) has not fully emerged from its envelope yet. In contrast, TW Hya (*middle panel*) is an old (∼10 Myr) T Tauri star. Other morphologies observed in the dust continuum are bright inner regions with much fainter outer regions. In the young disk V883 Ori (*right panel*) this transition has been suggested to be due to the water snowline. For reference, a 30-AU scale bar (the radius of Neptune's orbit) is shown in the lower right corner of each panel. Image credits: ALMA(ESO/NAOJ/NRAO); C. Brogan, B. Saxton (NRAO/AUI/NSF) – S. Andrews (Harvard-Smithsonian CfA); B. Saxton (NRAO/AUI/NSF); ALMA (ESO/NAOJ/NRAO) – L. Cieza et al.; ALMA (ESO/NAOJ/NRAO).

Onset of planet formation

Planet formation was originally thought to start in protoplanetary disks, after the envelope has dissipated. However, more and more studies are providing evidence that the first steps of planet formation already occur much earlier, in young disks that are still embedded. Characteristics of grain growth have been observed in protostellar envelopes (Kwon et al. 2009; Miotello et al. 2014), and recently in the embedded disk TMC1A (Harsono et al. 2018). The ALMA images of the young HL Tau disk suggest that even km-sized bodies may have formed before the envelope has fully dissipated (**Fig. 1.3**; ALMA Partnership et al. 2015), although subsequent studies have shown that rings are not necessarily the result of (young) planets (see e.g., the discussion and references in Huang et al. 2018).

Additional evidence for an early onset of planet formation is given by protoplanetary disk surveys: the majority of protoplanetary disks seem to have too little material to form the planetary systems that we observe (e.g., Ansdell et al. 2016; Manara et al. 2018). In contrast, young disks seem massive enough (Tychoniec et al. 2018, Tobin et al., in prep.). However, the picture of disk mass evolution may be more complicated as not all star forming regions follow the trend of decreasing median disk mass of more-evolved young stars (Cazzoletti et al. 2019; Williams et al. 2019). Furthermore, the dust opacity may be higher than assumed due to neglect of dust scattering (Zhu et al. 2019), which would mean that disk masses are underestimated.

Nonetheless, studies of our own Solar System also point to an early start of planet formation. The observed dichotomy in meteorite composition implies that two dust populations have been spatially separated in the disk for an extended period of time. The most plausible mechanism for this is that a forming Jupiter inhibited the inward drift of material from the outer regions, but this requires that Jupiter had already

grown beyond 20 Earth masses within a million years (Kruijer et al. 2017). Together, these results indicate that planet formation already starts in the embedded phase.

1.2 Chemistry during star and planet formation

The material in the local interstellar medium (ISM) consists primarily of hydrogen (H; 90% by number) and helium (He; 8% by number). The heavier elements are predominantly oxygen (O), carbon (C) and nitrogen (N), with solar abundances of 4.9×10^{-4}, 2.7×10^{-4} and 0.7×10^{-4} with respect to H, respectively (Asplund et al. 2009). Refractory species like magnesium (Mg), silicon (Si) and iron (Fe) are present in even lower amounts (a few times 10^{-5}), and are almost completely locked up in dust grains. Chemical processes during different stages of star formation convert the former volatile atoms into molecules with increasing complexity, possibly up to building blocks for life (see e.g., Herbst & van Dishoeck 2009; Caselli & Ceccarelli 2012 for a review). A molecule with more than six atoms, that contains carbon and hydrogen, is referred to as a *complex organic molecule* (*COM*).

Chemical processes during star formation can roughly be divided into two main types: reactions that occur in the gas phase, and reactions that take place on the surfaces of dust grains (see e.g., reviews by Tielens 2013; van Dishoeck 2014). A third category consists of processes that transfer atoms and molecules between the gas and solid phase. At the low tempertures ($\lesssim$ 100 K) characteristic for most stages of star formation, gas-phase chemistry is dominated by exothermic reactions (that is, reactions releasing energy) and reactions without an activation barrier. Most reactions are therefore either between a neutral molecule and a positively charged atom or molecule (ion-neutral reactions), or between a positively charged (molecular) ion and an electron (recombination reactions).

Dust grains are important to astrochemistry because they provide a surface area on which atoms and molecules can accrete, thereby enhancing the probability that species meet and react. This is, for example, crucial for the formation of the most abundant interstellar molecule, H_2. In addition, excess energy created by a reaction can be absorbed by the grain, whereas in the gas phase this has to be stored internally in the newly formed molecule, which may lead to immediate dissociation. Reactions on the grain surface include mainly hydrogen atoms and radicals, that is, atoms or molecules with unpaired electrons. Whether a species is present in the gas phase or on the grain surface (as ice) depends primarily on the temperature. These processes are referred to as *freeze-out* and *thermal desorption*. In addition, some species desorb from the grains upon impact of UV photons (photodesorption) and in other cases the excess energy released in a reaction may be used to transfer the newly formed molecule into the gas phase (chemical desorption).

The following sections give an overview of the main chemical processes during the different stages of star formation.

1.2.1 Dark cloud and dense core chemistry

Dark clouds are characterized by temperatures of roughly 10 K and densities in the order of 10^4–10^5 hydrogen nuclei cm^{-3}. Gas-phase chemistry is initiated by ionization of H_2 by cosmic rays leading to the formation of H_3^+. The reaction between H_3^+ and C, O and N atoms is followed by a chain of ion-molecule reactions creating a variety

of chemical species, with CO becoming the most abundant gas-phase molecule after H_2. A characteristic for molecules formed in the gas phase during this stage is that they tend to be very unsaturated, that is, each atom is not connected to the maximal possible number of other atoms. This is because the transfer of an H atom from H_2 to molecular ions is often endothermic (requires energy) or possesses an activation barrier and therefore does not occur at low temperatures. In addition, since reactions with C or C^+ often lead to carbon insertion at low temperatures, dark cloud chemistry produces many long carbon chains. Carbon chains up to C_8H, C_8H^-, HC_7O and HC_9N have been observed, for example, in the well-studied core TMC-1 (e.g., Kaifu et al. 2004; Cordiner et al. 2017). Recently, McGuire et al. (2018) reported the detection of the first aromatic molecule, benzonitrile (c-C_6H_5CN), toward this source.

Another characteristic of gas-phase chemistry in cold environments is a high level of deuterium (D) fractionation. Because the reaction between H_3^+ and HD, which produces H_2D^+ and H_2, is slightly exothermic, the reverse reaction of H_2D^+ and H_2 does not take place at temperatures below ∼30 K. This results in a significantly larger H_2D^+/H_3^+ abundance ratio and therefore deuterium fractionation (D/H abundance ratios up to ∼0.1) compared with the elemental D/H ratio (typically $\sim 2\times10^{-5}$; Linsky 2007) (Stark et al. 1999). Even doubly- and triply-deuterated molecules such as D_2CO (formaldehyde) and ND_3 (ammonia) have been detected (see Ceccarelli et al. 2014 for a review).

Freeze-out of atoms onto dust grains, followed by diffusion over the surface leads to efficient hydrogenation reactions producing large amounts of water ice (H_2O), and smaller amounts of methane (CH_4) and ammonia (NH_3; see e.g., reviews by Tielens & Hagen 1982; van Dishoeck et al. 2013; Linnartz et al. 2015). In addition, freeze-out of CO can result in the formation of CO_2 ice. In the densest, coldest inner region of dense cores, most of the CO will freeze out, creating a CO ice layer on top of the earlier formed water-dominated layer. Hydrogenation of CO will then result in the formation of formaldehyde (H_2CO) and methanol (CH_3OH), and more complex species (Watanabe & Kouchi 2002; Cuppen et al. 2009; Chuang et al. 2016) up to molecules as glycolaldehyde ($CH_2(OH)CHO$) and ethylene glycol (($CH_2(OH)_2$) (Fedoseev et al. 2015), even at temperatures as low as 10–15 K (see **Fig. 1.4**).

Ice observations through absorption bands of vibrational transitions in the near- to far-infrared have confirmed the layered ice structure and the formation of methanol on the grain surface, but the presence of more complex species is hard to infer from these observations (see Boogert et al. 2015 for a review). COMs like acetaldehyde (CH_3CHO), dimethyl ether (CH_3OCH_3) and methyl formate (CH_3OCHO) are also detected in the gas phase in cold dense cores (e.g., Bacmann et al. 2012; Cernicharo et al. 2012). This can not be explained by gas-phase chemistry alone, and thus requires non-thermal desorption processes such as photodesorption and chemical desorption to be active (e.g., Öberg et al. 2007; Minissale et al. 2016).

Massive freeze-out of CO in dense cores also influences the gas-phase chemistry, as this means that the main reactant of H_3^+ and H_2D^+ is removed from the gas phase. CO freeze-out therefore results in increased abundances of deuterated species and nitrogen-containing molecules like N_2H^+ and NH_3 (e.g., Caselli et al. 1999; Bergin et al. 2001). Freeze-out of H_2O in dense regions likely increases the abundance of HCO^+ (e.g., Phillips et al. 1992; Bergin et al. 1998).

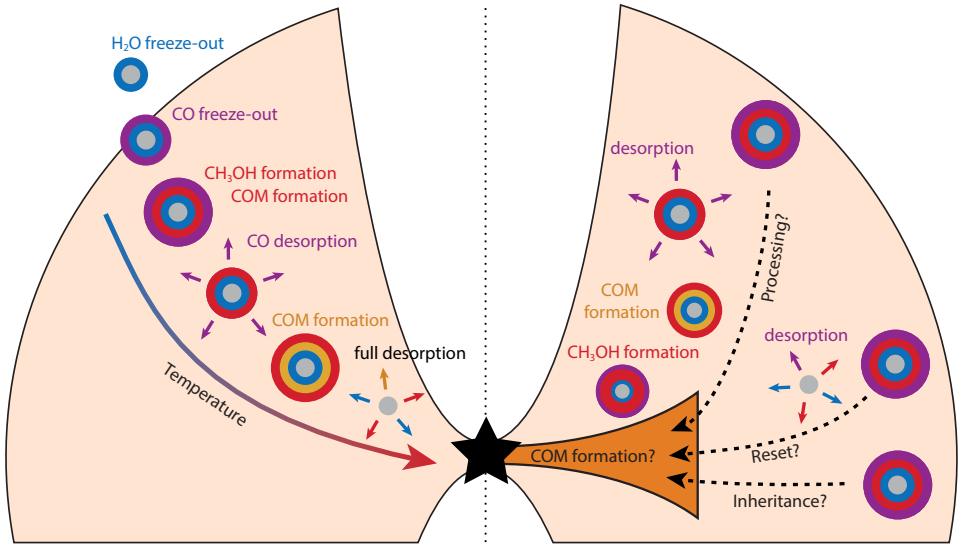

Figure 1.4: Schematic overview of some of the chemistry during low-mass star formation. The *left side* shows the build up of ices and the formation of complex organic molecules during core collapse and in the protostellar envelope. The *right side* illustrate three possible scenarios for the disk composition: full inheritance from the core, full reset into atoms, or processing of the core material (freeze-out, redesorption, formation of new species). How much each of these pathways contribute is still unclear, as well as whether COMs can form in the embedded disk.

1.2.2 Hot core chemistry

Once the protostar is formed it starts to heat up its surroundings. The first changes occur in the surface chemistry (Fig. 1.4). As soon as the grains become warmer than 20 K, H atoms reside for too short a time on the surface to be the dominant reactant and the most volatile species such as CH_4, CO and N_2 start to desorb. Cosmic ray-induced UV photons create radicals that can diffuse along the surface and react to create more complex species such as methyl formate (CH_3OCHO), dimethyl ether (CH_3OCH_3) and formic acid (HCOOH) (e.g., Garrod & Herbst 2006). Reactions involving radicals formed in these processes may even lead to formation of the simplest amino acid glycine (Garrod et al. 2008; Garrod 2013).

As the temperature further increases to 100–300 K, the ice mantles will fully sublimate and enrich the chemical complexity of the gas. At these temperatures, endothermic reactions and reactions with a barrier become efficient and the desorbed molecules were therefore thought to drive gas-phase chemistry (e.g., Charnley et al. 1992). However, a re-evaluation of reaction rate coefficients and branching ratios showed that gas-phase chemistry is less important than initially thought (e.g., Geppert et al. 2006) and that most of the complexity is produced in the ice. Meanwhile, the increasing strength of the protostellar radiation field could play an active role in molecular destruction.

Complex molecules are indeed readily detected toward these so-called *hot cores*, but with line surveys (in particular with ALMA) we are now starting to construct the full inventory for both low and high-mass sources (e.g., Jørgensen et al. 2016; Belloche

et al. 2016; Pagani et al. 2017, and see McGuire 2018 for an overview of all species detected so far and corresponding references). The largest number of COMs have been observed (for the first time) toward the high mass hot cores in Sagitarius B2, such as glycolaldehyde (CH_2OHCHO, a sugar-like molecule), acetamide (CH_3CONH_2, the largest interstellar molecule with a peptide bond) and amino acetonitrile (NH_2CH_2CN, a direct precursor of the amino acid glycine). Glycolaldehyde has now also been detected on the scale of planetary systems toward the low mass protostar IRAS 16293B (Jørgensen et al. 2012). Other detections worth mentioning are the observations of propylene oxide (CH_3CHCH_2O, the first chiral molecule; chirality is a characteristic of many biomolecules) and iso-propyl cyanide (i-C_3H_7CN, the first non-linear carbon chain).

However, one of the main surprises of the WISH program (Water In Star-forming Regions with the *Herschel Space Observatory*) was that only very little of the water emission toward protostellar envelopes actually originates in the hot core region (instead, most of the emission traces shocked gas; see e.g., van Dishoeck et al. 2011). Spatially resolved interferometer observations did find warm $H_2^{18}O$ emission towards three hot cores, but with low abundances between 10^{-8} and a few times 10^{-6} (Jørgensen & van Dishoeck 2010; Persson et al. 2012, 2014). In comparison, thermal evaporation of water at $T \gtrsim 100$ K is expected to produce a gas-phase water abundance of 10^{-4}. A caveat is that the observed abundances are calculated based on a spherical envelope model. Taking into account that a disk can be present in the inner most region increases the derived abundances by ∼1 order of magnitude, still a few orders of magnitude below what is expected for two of the sources (Persson et al. 2016). Low water abundances could be the result of destruction by X-rays (Stäuber et al. 2006), or maybe the sequestering of water as ice in larger grains that does not desorb.

Another unexpected discovery was the detection of several carbon chains toward the protostar L1527 (see review by Sakai & Yamamoto 2013), as these species are characteristic of dark cloud chemistry. The authors suggest that this may be distinctive for sources where the temperature did not rise above ∼30 K during the collapse. Such temperatures allow for CH_4 ice desorption, and the subsequent gas-phase formation of carbon chains, while the more complex species remain frozen out. However, models show that when carbon chains are formed at ∼30 K, they do not disappear rapidly from the gas as the temperature reaches 200 K. In addition, carbon chains are also abundant in UV-irradiated outflow cavity walls (e.g., Murillo et al. 2018). These observed morphologies could thus also be due to a combination of the source physical structure and the region predominantly probed by the observations.

1.2.3 Protoplanetary disk chemistry

After the envelope has dissipated, a protoplanetary disk remains. Radial and vertical gradients in temperature (due to heating by the central star) and density cause a layered chemical structure in these disks (**Fig. 1.2**; Aikawa et al. 2002, and the review by Dutrey et al. 2014). In the surface layers, molecules are photodissociated and atoms ionized by the UV radiation and in the cold midplane most molecules are frozen out. At intermediate heights (warm molecular layer), the dust grains are warm enough to prevent complete freeze-out and the UV radiation is sufficiently attenuated for molecules to survive, but still strong enough to drive an active ion-molecule chemistry.

Many small molecules and isotopologues (that is, molecules with a less abundant ^{13}C, ^{18}O, ^{17}O or ^{15}N isotope) have been observed in disks, and the resolution and sensitivity provided by ALMA allows to resolve structures (see e.g., a recent overview by Bergin & Cleeves 2018). Small surveys are now being conducted toward the brightest disks, but so far the overall conclusion seems that there is a great diversity between disks (e.g., Thi et al. 2004; Huang et al. 2017).

In contrast to small molecules, only few complex species have been detected in disks. COMs desorb from the dust grains at temperatures $\gtrsim$100–150 K, and are thus frozen out except in the inner few AU and possibly the surface layers. Gas-phase formation routes or non-thermal desorption processes are thus required to get observable amounts in the gas phase. The first disk COM to be detected was methyl cyanide (CH_3CN; Öberg et al. 2015b), which has currently been observed in six disks (Bergner et al. 2018; Loomis et al. 2018). Methanol (CH_3OH) has only been detected in TW Hya (Walsh et al. 2016) and very deep upper limits were presented for HD163296 (Carney et al. 2019), suggesting that disk chemistry can be strongly influenced by the stellar type. Formic acid (t-HCOOH) is the third organic molecule larger than formaldehyde (H_2CO) that is detected in disks, but again, so far only in TW Hya (Favre et al. 2018). These observations show that it is very challenging to probe the chemical complexity of the protoplanetary disk material.

A current topic of debate is the abundance and fate of CO in protoplanetary disks. Because the most abundant molecule, H_2, does not have a dipole moment, it cannot be observed at millimeter wavelengths. Its deuterated counterpart, HD, can be observed in the far-infrared, but not with presently available instruments. The readily observable, second most abundant molecule, CO, is therefore generally used as a tracer of the disk gas mass. However, a comparison between the CO-derived gas mass and the HD-derived gas mass for the three disks with HD detections by the *Herschel Space Observatory* showed that the HD masses are a factor five to two orders of magnitude higher than the CO masses (Favre et al. 2013; McClure et al. 2016). CO seems thus depleted, on top of freeze-out and photodissociation (Kama et al. 2016; Schwarz et al. 2016). Low CO-based gas masses are also observed for the disks in the ALMA survey of the Lupus star forming region (Ansdell et al. 2016; Miotello et al. 2017), suggesting this may be the result of a common process. Independent evidence for CO depletion comes from observations of bright C_2H and c-C_3H_2 emission, species expected to be especially abundant when both carbon and oxygen are depleted with a gaseous C/O ratio >1 (Kastner et al. 2015; Bergin et al. 2016). A possible explanation can be that gaseous CO is turned into more complex species, that subsequently freeze-out, through reactions with He^+ (e.g., Aikawa et al. 1999; Bergin et al. 2014; Schwarz et al. 2018). Alternatively, CO can be converted into less volatile species in the ice (e.g., Bosman et al. 2018). A third possibility is that CO is locked up in large icy grains that reside in the midplane and cannot diffuse upward into layers where CO can desorb (e.g., Krijt et al. 2018). These processes are time dependent; young disks are therefore expected to have less CO depletion.

Snowlines

As described above, protoplanetary disks are characterized by a large cold midplane region where most molecules are frozen out. The midplane radius where a molecule becomes more abundant in the ice than in the gas phase is called a *snowline*. The temperature at which freeze-out occurs depends on a species-specific binding energy

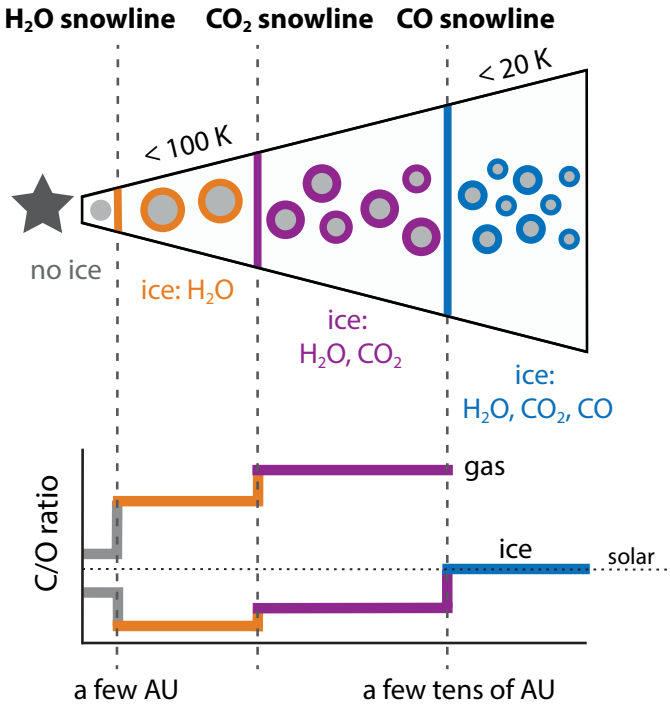

Figure 1.5: Schematic overview of the major snowlines and their expected location in protoplanetary disks (*top*). For simplicity, the snowlines are marked as vertical lines instead of snow surfaces (see Fig. 1.2). The sequential freeze-out of these dominant carbon and oxygen carriers results in a radial gradient in the elemental C/O ratio of the planet-forming material (*bottom*; adapted from Öberg et al. 2011).

to the (icy) dust grains. The radial temperature gradient in protoplanetary disks therefore results in sequential freeze-out of volatile molecules (Fig. 1.5). Because of the vertical temperature gradient within disks, the region where a molecule is frozen out is bounded by a *snow surface* (see Fig. 1.2).

Snowlines, and especially the water snowline, play an important role in planet formation (as described in Sect. 1.1.3) as dust growth is enhanced near these freeze-out zones (e.g., Stevenson & Lunine 1988; Schoonenberg & Ormel 2017). Snowlines were therefore postulated as a mechanism to create rings and gaps in protoplanetary disk dust emission (e.g., Zhang et al. 2015; Pinilla et al. 2017). However, high resolution observations with ALMA of a large number of protoplanetary disks show no correlation between the gap locations and the CO_2, CO and N_2 snowlines (van Terwisga et al. 2018; Long et al. 2018; Huang et al. 2018; van der Marel et al. 2019). Effects on grain growth may thus be limited to the water snowline.

In addition to planet formation, snowlines strongly affect the chemical composition of planets. The selective freeze-out of major carbon or oxygen carrying species at different snowlines causes the elemental C/O-ratio of the planet-forming material to vary with radial distance from the star (Fig. 1.5; Öberg et al. 2011; Eistrup et al. 2018). The bulk composition of planets may therefore be regulated by their formation location with respect to the major snowlines (e.g., Madhusudhan et al. 2014; Walsh

et al. 2015; Cridland et al. 2017).

The most important snowline is the water snowline, because of its role in planet formation and because water ice contains the bulk of the ice mass and oxygen budget. Observing the water snowline in protoplanetary disks, however, is very challenging. First, the snowline is located only a few AU from the star due to the high desorption temperature of water of ∼100–150 K. This means that an angular resolution of ∼0.01″ is required to resolve the snowline location in disks around Sun-like stars in the nearest star-forming region Taurus. Second, the only suitable thermal water lines observable from the ground are those from the ∼500 times less abundant isotopologue $H_2^{18}O$. High sensitivity is thus required as well, and as such, no detection has yet been made (e.g., Notsu et al. 2019). The only disk for which an indirect measurement of the water snowline location has been reported is V883 Ori (Cieza et al. 2016). This young star is undergoing an accretion burst, which heats the disk and shifts the snowline outward. An abrupt change in the continuum intensity corresponding to a change in the optical depth is observed around ∼40 AU. Such effect is expected around the water snowline. However, direct molecular line observations are required to confirm the snowline location (see also **Chapter 7**).

Another interesting snowline is the CO snowline, because CO ice is the starting point for the formation of many complex organics (see **Sect.1.2.1**). Moreover, the low desorption temperature (∼20–30 K) places this snowline far enough from the star (10s–100 AU) to be spatially resolved with ALMA. However, CO line emission is generally optically thick, even for the less abundant isotopologues ^{13}CO and $C^{18}O$, and originates in the disk surface layers. The very rare isotopologue $^{13}C^{18}O$ is therefore required to probe the midplane (Zhang et al. 2017), but its low abundance restricts observations to the nearest and brightest disks. An alternative approach is to observe molecules whose abundance is strongly affected by the freeze-out of CO. Examples of such molecules are DCO^+, N_2H^+ and N_2D^+ (**Fig. 1.6**).

DCO^+ emission is expected to originate in a ring just inside the CO snowline, where the temperature is low enough such that H_2D^+ is abundant, but there is still enough gaseous CO left to form DCO^+ (**Fig. 1.6**). Ring-shaped DCO^+ emission was indeed observed toward HD163296 and IM Lup (**Fig. 1.6**; Mathews et al. 2013; Öberg et al. 2015a). However, for HD163296, it was later shown that the outer radius does not correspond to the CO snowline (Qi et al. 2015); probably because DCO^+ can also form in warmer disk layers ($T \gtrsim 70$ K) through reaction with CH_2D^+ (Favre et al. 2015). Although DCO^+ emission does not seem to have a direct correlation with the CO snowline, detailed modeling including an appropriate physical structure for the target disk can narrow down the snowline location (Carney et al. 2018).

N_2H^+ (and N_2D^+) emission is also expected to be ring-shaped, but with the inner edge around the CO snowline because N_2H^+ can only be abundant when CO is frozen out (**Fig. 1.6**). N_2H^+ has indeed be used to locate the CO snowline in TW Hya and HD163296, at radii of 30 and 90 AU, respectively (**Fig. 1.6**; Qi et al. 2013b, 2015). These studies also highlight the importance of locating the snowline based on molecular emission, as the snowline radius corresponds to a temperature of ∼17 K in TW Hya and ∼25 K in HD163296. This difference could be due to different ice compositions in the two disks. However, these snowline radii are likely upper limits (that is, maximum distances from the star), because chemical modeling shows that the N_2H^+ abundance and emission peak outside, instead of directly at the snowline (Aikawa et al. 2015 and **Chapter 2**). For TW Hya, this is consistent with the $^{13}C^{18}O$ observations (Zhang et al.

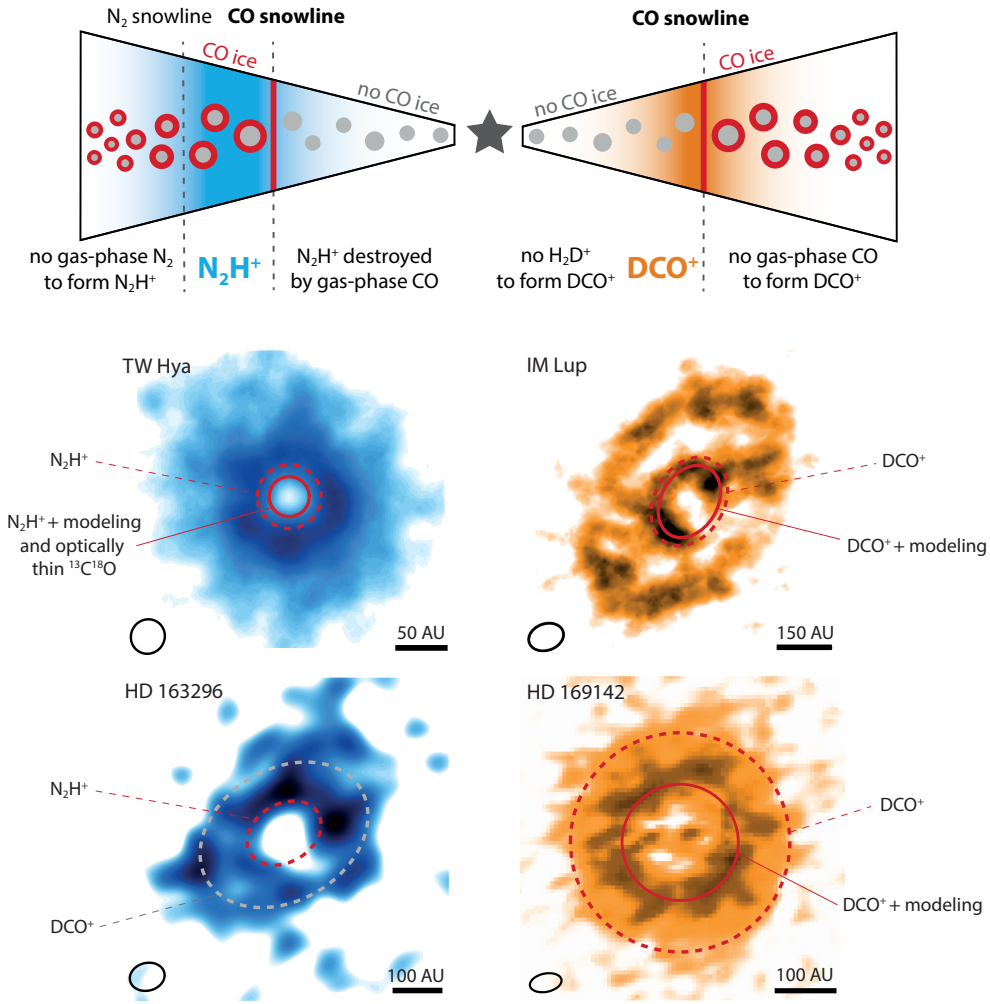

Figure 1.6: Schematic overview of the expected relation between the CO snowline and N_2H^+ (blue; *top left panel*) or DCO^+ (orange; *top right panel*) based on simple chemical considerations. ALMA observations of N_2H^+ and DCO^+ in protoplanetary disks are shown in the *middle* and *bottom left panels*, and *middle* and *bottom right panels*, respectively. The corresponding expected CO snowline locations are marked with a red dashed contour. However, based on both chemical modeling (**Chapter 2**) and $^{13}C^{18}O$ observations, the snowline is located at smaller radii in TW Hya (solid red contour). In HD 163296, a comparison between the snowline location based on N_2H^+ and DCO^+ (dashed gray contour) revealed that the snowline derived from N_2H^+ is in better agreement with the snowline location based on $C^{18}O$ observations. Modeling of the DCO^+ emission in IM Lup and HD 169142 also places the snowline closer in than the outer edge of the DCO^+ emission due to the contribution of a warm DCO^+ formation route. The outer DCO^+ ring in IM Lup may be due to photodesorption of CO in the outer disk or temperature inversion. Images are adapted from Qi et al. (2013b, 2015), Mathews et al. (2013), Öberg et al. (2015a) and Carney et al. (2018).

2017). In addition, Chapter 2 predicts that N_2H^+ can be abundant as well in a surface region of the disk and this has very recently been confirmed by observations (Schwarz et al. 2019).

1.2.4 Chemical composition of comets

Comets are likely formed in the cold outer part of the disk from which the Solar System formed. Assuming that comets have undergone no major processing since their formation, their chemical composition is a direct window to the composition of the outer disk. In addition, comets may have seeded the young Earth with water and prebiotic molecules. Space missions to comets therefore provide valuable information on our origins. A review on cometary abundances is given by Mumma & Charnley (2011) and Bockelée-Morvan et al. (2015), and here a few interesting, more recent results from the *Rosetta* mission to comet 67P/Churyumov-Gerasimenko (67P/C-G) are highlighted (Altwegg et al., in press). An exciting result is the detection of the simplest amino acid, glycine (Altwegg et al. 2016), confirming the earlier detection in comet Wild 2 by the *Stardust* mission (Elsila et al. 2009). Together with the detection of phosphorus and many organic molecules, the *Rosetta* results demonstrate that comets could have played a key role in the emergence of life. A surprise was the detection of a high abundance of molecular oxygen (O_2) in the cometary coma (Bieler et al. 2015), suggesting that the O_2 is incorporated during the comet's formation. Chemical models show that the O_2 has to have formed during the dark cloud stage and survived the transport into the disk. This does require slightly warmer cloud conditions ($\sim$20 K) than generally assumed for other dark clouds (Taquet et al. 2016a). Re-analysis of the *Giotto* results demonstrate that O_2 is present in comet 1P/Halley at a similar level as in 67P/C-G ($\sim$4% with respect to H_2O; Rubin et al. 2015).

1.3 Chemistry as a thermometer

Molecular line observations are indispensable for studying star and planet formation. Not only do they provide information on the chemical composition of the planetary building blocks, they are also excellent tracers of the kinematics and physical conditions in the star- and planet-forming environment. There are several ways in which molecular line emission can be used as a temperature probe:

Direct observations of freeze-out

The most intuitive way in which molecules react to temperature is that they freeze out from the gas phase onto the dust grains when the temperature falls below their freeze-out temperature. Since this temperature is species specific (Fig. 1.5), with only a small density dependence, the absence of a certain molecule can constrain the temperature to below its freeze-out temperature. For example, the region in the disk midplane where CO is absent has a temperature below $\sim$20–25 K, and regions with emission from water or complex organics have temperatures $\gtrsim$ 100–150 K. However, this can only be applied when there is a direct line of sight to the region of interest. CO freeze-out is often impossible to see directly in protoplanetary disks because the emission becomes optically thick in the warmer surface layers where CO is not frozen out. Only when the disk is seen edge on can the midplane, and thus CO freeze-out, be observed directly (e.g., Dutrey et al. 2017).

Chemical effects due to freeze-out

Freeze-out of molecules can also affect other molecules through chemical reactions that can only happen in absence or presence of the frozen out molecule. Examples of such chemical tracers are N_2H^+, N_2D^+, HCO^+ and DCO^+. As outlined in Sect. 1.2.3 (see Fig. 1.6), N_2H^+ and N_2D^+ trace the region where CO is frozen out because these molecules are otherwise destroyed by gaseous CO. Since CO is the main reactant of H_3^+, the absence of CO increases the amount of H_2D^+ and therefore the amount of DCO^+. However, CO is also the parent molecule for DCO^+. DCO^+ therefore traces the region where CO starts to freeze out. HCO^+ is sensitive to the freeze-out of water, because water is the main destructor of HCO^+. Simple chemical models, that is, including only the main reactions for formation and destruction of either N_2H^+, N_2D^+, HCO^+ or DCO^+, in combination with radiative transfer (see Sect.1.3.2) can be used to derive the CO and H_2O freeze-out region.

Rotation diagrams

Rotational energy levels of molecules can be populated (excited) through collisions with other molecules, usually H_2, and depopulated (de-excited) through both collisions and the spontaneous emission of a photon. When the density of the collision partner is high enough for the collisional excitation to balance the spontaneous de-excitation (that is, above the so-called critical density), the level populations are thermalized such that they follow a Boltzmann distribution for a given gas kinetic temperature. This is called local thermodynamic equilibrium (LTE). If a molecule is in LTE, and multiple lines are observed, its excitation temperature and column density can be well-constrained through a rotation diagram (e.g., Goldsmith & Langer 1999). For such analysis, the column density of molecules in the upper state, N_u, is calculated for each transition using the observed integrated flux density $S_\nu \Delta v$:

$$N_u = \frac{4\pi S_\nu \Delta v}{A_{ul} \Omega h c}, \tag{1.1}$$

where A_{ul} is the Einstein A coefficient and Ω is the solid angle subtended by the source. The upper state level column density can be related to the total column density, N_T, by the Boltzmann equation:

$$\frac{N_u}{g_u} = \frac{N_T}{Q(T_{\rm rot})} e^{-E_u/kT_{\rm rot}}, \tag{1.2}$$

where g_u and E_u are the degeneracy and energy of the upper state level, respectively, Q is the molecular partition function and $T_{\rm rot}$ is the rotational temperature. Taking the logarithm then allows for determining $T_{\rm rot}$ and N_T through a linear least squares regression:

$$\ln \frac{N_u}{g_u} = \ln N_T - \ln Q(T_{\rm rot}) - \frac{E_u}{kT_{\rm rot}}. \tag{1.3}$$

If a line is not optically thin, the upper level column density must be multiplied by a correction factor, C_τ:

$$C_\tau = \frac{\tau}{1 - e^{-\tau}}, \tag{1.4}$$

where τ is the line optical depth. If $T_{\rm rot}$ is known, the column density can also be estimated from a single line observation.

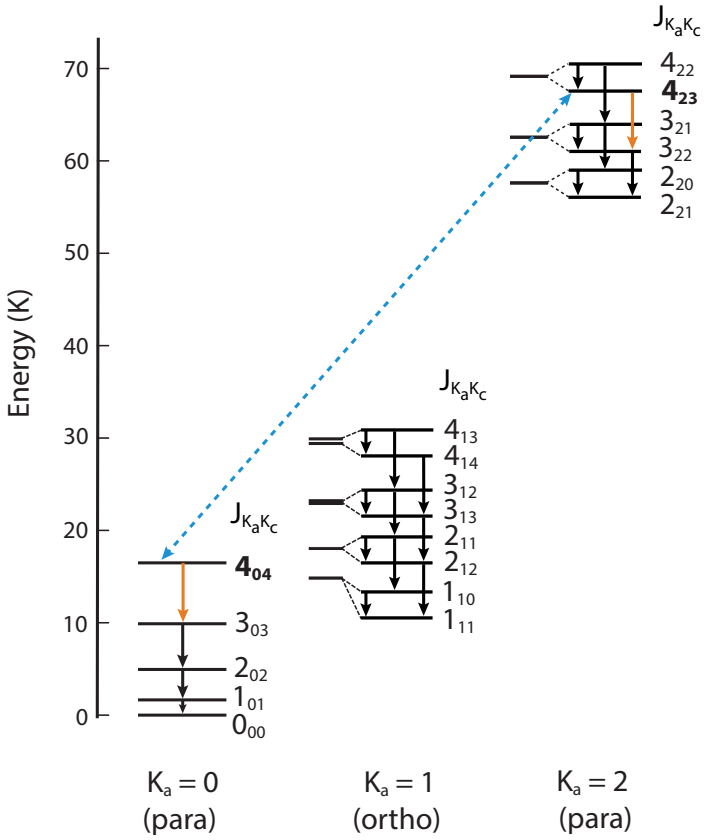

Figure 1.7: Energy level diagram for thioformaldehyde (H_2CS) for levels up to $J = 4$ and $K_a = 2$. Radiative transitions (solid arrows) are only allowed within a K_a ladder. No transitions are allowed between ortho and para states, but collisional excitation and de-excitation is possible between all para states, and all ortho states. Line ratios between two transitions with a different K_a state (for example the $4_{23} - 3_{22}/4_{04} - 3_{03}$ ratio; orange arrows) are good temperature tracers because only collisional transitions are possible between the 4_{04} and 4_{23} level (blue dashed arrow). Their ratio is therefore determined by temperature.

Temperature-dependent line ratios

The relative strength of transitions that can only be populated and depopulated by collisions is a good measure of temperature, since collision rates are determined by temperature. Formaldehyde (H_2CO) and thioformaldehyde (H_2CS) have such transitions (e.g., Mangum & Wootten 1993; van Dishoeck et al. 1993, 1995). These slightly asymmetric rotor molecules have their energy levels designated by the quantum numbers J, K_a and K_c (Fig. 1.7). Line ratios involving different K_a ladders are good tracers of the kinetic temperature because transitions between energy levels with different K_a values are radiatively forbidden and thus take place only through collisions. Transitions with the same ΔJ are closely spaced in frequency, and can therefore often be observed within one frequency tuning. This eliminates calibration uncertainties in the line ratio.

1.3.1 Molecular line observations

Both high angular resolution and high sensitivity are required for molecular line observations in (embedded) disks. Therefore, ALMA is the best instrument for such studies. ALMA is a (sub)millimeter wavelength interferometer and consists of 66 antennas located at an altitude of 5000 meters on the Chajnantor plateau in the Atacama desert, Chile. Fifty 12-m antennas make up the main array, that can cover baselines of maximum ∼150 m in the most compact configuration and up to ∼16 km in the most extended configuration. This corresponds to angular resolutions between 1.5″ and 0.018″ at 230 GHz (1.3 mm). In addition, twelve 7-m antennas form the Atacama Compact Array (ACA), with baselines up to 45 meters (5.4″ resolution at 230 GHz), and four 12-m antennas are used for total power observations. Currently, eight of the ten receiver bands are operational, covering frequencies from 84 to 950 GHz (with the exception of a few frequency ranges with strong atmospheric absorption). The maximum spectral resolution is 31 kHz and the total amount of bandwidth covered in one spectral setting depends on the requested spectral resolution with a maximum of 8 GHz at the lowest spectral resolution (0.976 MHz).

Other operational (sub)millimeter interferometers are the Submillimeter Array (SMA) in Hawaï and the NOrthern Extended Millimeter Array (NOEMA) in France. The SMA consists of eight 6-m dishes covering baselines of maximum 509 meters and frequencies from 180 to 420 GHz. NOEMA is an extension of the Plateau de Bure Interferometer (PdBI), with currently ten 15-m antennas covering baselines up to 760 meters (0.5″ resolution at 230 GHz) and frequencies between 76 and 274 GHz. With fewer antennas and shorter baselines, these observatories cannot reach the angular resolution and sensitivity of ALMA. However, upgrades of the receivers allow for much larger spectral coverage in one setting. In addition, with their location on the Northern hemisphere, they are more suited for observing high-declination sources, such as Perseus, than ALMA. Most observations in this thesis are done with ALMA, whereas NOEMA observations are used in **Chapter 5**.

Interferometers do not observe the sky brightness of a source directly, but instead measure the interference pattern of each pair of antennas (*visibilities*). The sky brightness distribution can then be retrieved by a Fourier transform of the visibility function. The more baselines with different length and orientation, the more the so-called *uv*-plane gets filled, and the more reliable the image that is reconstructed. The number of baselines equals the number of permutations of pairs of antennas. In addition, due to the Earth's rotation, the orientation of the baselines changes as seen from the source, which helps filling in the *uv*-plane. Calibration, that is, correcting for atmospheric variations, non-uniform response across the receiver bands and total flux measured, and imaging of ALMA data is done with the Common Astronomy Software Applications (CASA; McMullin et al. 2007). For NOEMA data, the software package GILDAS[2] is used.

1.3.2 Radiative transfer

To interpret molecular line observations, physical and chemical models with different levels of complexity can be used. Subsequently, a radiative transfer model is employed to produce a synthetic image of the line emission. The three software packages used

[2]http://www.iram.fr/IRAMFR/GILDAS

in this thesis are RADEX, RATRAN and LIME (van der Tak et al. 2007, Brinch & Hogerheijde 2010, and Hogerheijde & van der Tak 2000, respectively). RADEX is a one-dimensional non-LTE code that assumes an isothermal and homogeneous medium. This assumption limits the number of free parameters and reduces the computational time. In the non-LTE situation, the molecular level populations depend on the radiation field, which in turn, depends on the level populations. RADEX uses the "escape probability method" to decouple the radiative transfer calculations from the calculations of the level populations (e.g., Sobolev 1960). This approach considers the probability that a photon will escape the medium, which depends on the optical depth of the transition. The publically available version of RATRAN deals with spherically symmetric geometries of varying temperature and density. In this case the radiation field and level populations have to be solved iteratively as functions of depth into the cloud. Finally, LIME (LIne Modeling Engine) works in arbitrary, three-dimensional geometries using a random grid in which the spacing of the grid cells can be weighted by, for example, density. LIME can be used for both LTE and non-LTE calculations. All codes require molecular collision rates for non-LTE calculations, many of which are collected in the Leiden Atomic and Molecular Database (LAMDA; Schöier et al. 2005).

1.4 Studies of embedded disks

Embedded disks are a critical stage, providing the link between the warm inner envelope and cold protoplanetary disk, and the initial conditions for planet formation. However, observational studies of embedded disks have long been hampered by a lack of spatial resolution and sensitivity of existing facilities. The presence of a disk can be derived from unresolved continuum fluxes at different wavelengths, but molecular line observations at high spatial resolution are needed to establish whether such structure is in fact a rotationally supported disk. High spatial and high spectral resolution are also necessary to disentangle emission from the disk and envelope. Line observations, however, require a much longer integration time than continuum observations because the emission covers a very narrow frequency range. ALMA now provides the sensitivity and resolution to study the physical and chemical conditions in embedded disks. The following sections provide a brief overview from early observations to the current ALMA studies.

1.4.1 Identification of protostars

Theoretically, the different phases of star formation are divided into four *Stages*, based on age, stellar mass and infall rate (as described in Sect. 1.1 and Fig. 1.1). Since these parameters are not always directly observable, young stellar objects (YSOs) are divided into different *Classes* based on observations. The dust around a YSO heats up by absorbing the high-energy (UV and optical) radiation from the star and accretion, and subsequently re-emits lower-energy radiation at longer wavelengths. YSOs, except for the most deeply embedded protostars, are therefore best identified at infrared to submillimeter wavelengths. The *Spitzer Space Telescope* had the sensitivity to detect YSOs down to the brown dwarf limit, and several large programs have been carried out at 3–160 μm to identify YSOs in several nearby molecular clouds (e.g., Evans et al. 2009; Dunham et al. 2013, 2015). Many of these regions have also been observed

at far-infrared wavelengths (55–670 μm) with the *Herschel Space Observatory* (e.g., André et al. 2010).

Lada (1987) used the infrared spectral index (the slope of the spectral energy distribution; the SED) between 2 and 10–60 μm to distinguish three groups of YSOs: *Class I, II* and *III* (Fig. 1.1). Greene et al. (1994) added a fourth class, the "*Flat-spectrum*" sources, and *Class 0* was added for protostars too deeply embedded to detect in the near-infrared (André et al. 1993). Other criteria are the ratio of submillimeter ($\lambda \geq 350\mu$m) to bolometric luminosity ($L_{\rm submm}/L_{\rm bol}$) and the bolometric temperature ($T_{\rm bol}$). The observed Classes roughly correspond to the theoretical Stages, but the difficulty is that the SED, and thus the parameters used to categorize objects into Classes, is sensitive to the geometry of the protostellar system (e.g., Crapsi et al. 2008). For example, $T_{\rm bol}$ can cross at least one Class boundary as the inclination changes from edge-on to face-on. In addition, $T_{\rm bol}$ may place an object in a different Class than $L_{\rm submm}/L_{\rm bol}$. One should thus keep in mind, when studying evolutionary trends, that observed Classes not necessarily correspond to physical Stages.

The large number of YSOs detected with *Spitzer* allowed for a statistical study of the lifetime of different Classes. By assuming a Class II lifetime of 2 Myr, and scaling this to the relative number of YSOs in other Classes, the protostellar lifetime (Class 0 + I) is ∼0.5 Myr (e.g., Dunham et al. 2014). This method does not take into account that star formation is sequential, that is, the current population of Class II sources comes from an earlier generation of Class 0, I and Flat sources. Kristensen & Dunham (2018) propose a different analysis to overcome this and find that YSOs spend on average ∼10% of their time in the embedded phase (Class 0 + I + Flat) and the remaining 90% of their time as Class II and III objects.

These surveys also confirmed earlier results that the observed protostellar luminosities are generally ∼10 times lower than expected based on accretion (e.g., Kenyon et al. 1990; Kenyon & Hartmann 1995; Young & Evans 2005; Evans et al. 2009). One solution for this "protostellar luminosity problem" is *episodic accretion*. In the episodic accretion scenario, the accretion process is variable and consists of short bursts of very rapid accretion as those observed for FU Ori objects (see e.g., reviews by Audard et al. 2014; Hartmann et al. 2016). A way to infer the occurence of such bursts observationally is with the radial extent of CO emission in a protostellar envelope. More extended emission than expected from the current luminosity indicates that the circumstellar material has recently been heated, evaporating the CO ice. Small surveys imply that a protostar undergoes approximately five bursts (e.g., Jørgensen et al. 2015).

1.4.2 Embedded disk studies before ALMA

Early studies of embedded disks focused on modeling the infrared and (sub)millimeter continuum SEDs of protostars using a theoretical density profile and radiative transfer codes. The first realistic SED models of protostars with an infalling envelope were computed by Adams et al. (1987) based on a one-dimensional rotating collapsing envelope model (Ulrich 1976; Cassen & Moosman 1981; Terebey et al. 1984) with a protostellar disk inside the centrifugal radius (that is, the radius at which the gravitational force is balanced by the centrifugal force). Whitney et al. (2003) improved upon these models by adding a flared accretion disk and bipolar cavities. For many sources a disk was required in order to obtain a reasonable fit (e.g., Kenyon et al. 1993). However, outflow opening angle, inclination, infall rate and centrifugal radius are degenerate in

SED fitting. Some of these parameters can be constrained from images (for example scattered light images; e.g., Eisner et al. 2005), and a more accurate description can be obtained by including the velocity structure as measured through molecular lines (e.g., Hogerheijde & Sandell 2000).

The advent of (sub)millimeter interferometry allowed studies of the colder mm-sized dust in disks at scales down to a few hundred AU. In interferometric observations, the physical scale probed scales inversely with the distance between two telescopes, so-called *baselines*. The longest baselines are most sensitive to disk emission, while shorter baselines probe the inner envelope. Since two telescopes cannot be infinitely close together, emission from the largest physical scales will always be filtered out. (Sub)millimeter interferometry is therefore well suited to distinguish the disk from the envelope. Moreover, at (sub)millimeter wavelengths, the dust is expected to be mostly optically thin and can therefore be used to calculate disk masses.

Small surveys (e.g., Looney et al. 2000; Jørgensen et al. 2009; Maury et al. 2019) and studies of individual sources (e.g., Hogerheijde 2001; Harvey et al. 2003; Enoch et al. 2009a) show that disks with radii of a few hundred AU and masses of a few times 0.01–0.1 $M_\odot$ are present in the embedded phase. But there are also sources where no massive extended disk is observed (e.g., Jørgensen 2004; Maury et al. 2010). Tobin et al. (2016b) performed the first complete survey of all protostars in a single star forming region using the Very Large Array (the VLA Nascent Disk and Multiplicity (VANDAM) survey). From these observations, 33% of the Class 0 protostars and 11% of the Class I protostars show a dust disk at 12 AU diameter resolution (Segura-Cox et al. 2018). Since 8 mm observations trace a population of larger dust grains, which have likely drifted toward the star, these data provide only lower limits to the disk size. Large disks (>100 AU) are thus possible during the embedded phase, although they do not seem to be common.

Although compact, disk-like continuum emission is prevalent in the Class 0 and I phase, molecular line observations are required to determine whether these structures are in fact rotationally supported. Furthermore, disks can be significantly larger in the gas than in the dust. Molecular line observations require much higher sensitivity than continuum observations, and in addition, high angular and spectral resolution are needed to distinguish true Keplerian rotation ($v_{\rm rot} \propto r^{-0.5}$) from rotation due to infall with angular momentum conservation ($v_{\rm rot} \propto r^{-1}$) (see e.g., Lee et al. 2009). Pre-ALMA interferometric line observations in combination with detailed radiative transfer modeling made it possible to constrain the radial distribution of molecular abundances and enabled studies of the kinematic structure of protostellar systems (e.g., Jørgensen et al. 2005). Such studies revealed a number of rotationally supported Class I disks based on HCO^+ emission (e.g., Brinch et al. 2007; Lommen et al. 2008) or emission from CO isotopologues (e.g., Takakuwa et al. 2012; Harsono et al. 2014). A kinematic analysis also allowed the mass of the protostar to be derived. Class 0 disks are harder to study because of the more massive envelope, but Tobin et al. (2012b) detected Keplerian rotation out to $\sim$ 150 AU in the Class 0 disk L1527 (**Fig. 1.8**). Large Keplerian disks (R >100 AU) are thus clearly present in Class I objects, and there is some evidence for large disks in Class 0 systems.

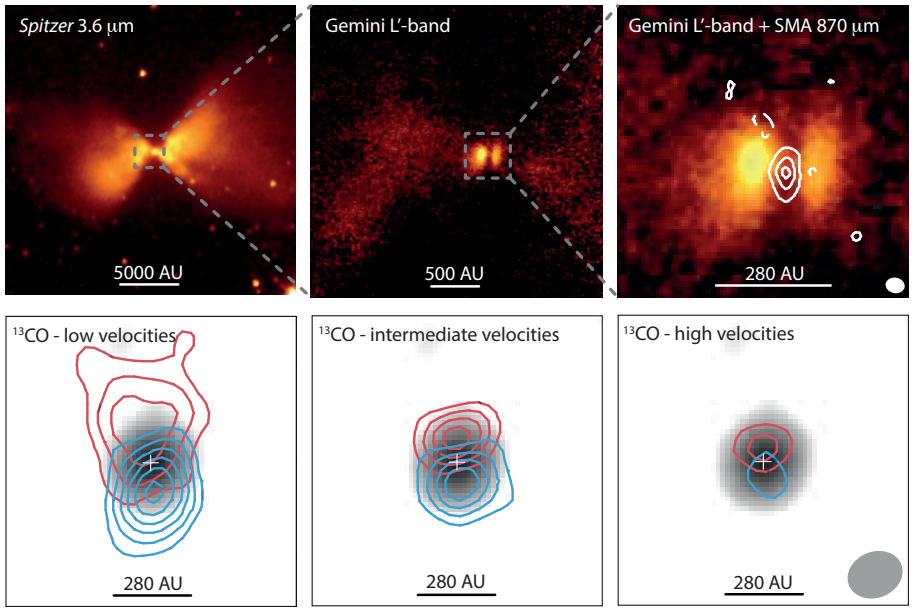

Figure 1.8: The first rotationally supported disk around a Class 0 protostar was detected around L1527 IRS in Taurus (Tobin et al. 2012b). The *Spitzer* IRAC 3.6 μm image shows the outflow cavities in scattered light (*top left panel*). The point-like structure in the center of the envelope is resolved into a bipolar scattered light nebula in the Gemini L$'$ image (*top middle* and *top right panel*). The dark lane is the shadow of the disk, which becomes visible in the 870 μm SMA image (white contours in *top right panel*). Keplerian rotation was established using ^{13}CO CARMA observations. The *bottom panels* show the integrated blueshifted (blue contours) and redshifted (red contours) emission at different velocity ranges overlaid on the CARMA 1.3 mm image. Images are adapted from Tobin et al. (2010, 2012b, 2013b).

1.4.3 Embedded disk studies with ALMA

With the higher sensitivity and spatial resolution of ALMA, continuum observations at wavelengths of ∼1 mm can be done routinely at subarcsecond resolution (∼one minute per source), and disk-like structures in continuum emission are ubiquitiously detected in surveys of embedded sources in ρ Ophiuchus and Orion (Williams et al. 2019; Tobin et al. in prep.). Both studies show that the disk mass decreases from Class 0 to Class II, consistent with the VLA results for Perseus (Tychoniec et al. 2018) and expectations from disk evolution. From the 328 protostars in Orion, 70 objects have disks with dust radii larger than 50 AU. There is a slight decrease in median disk radius for Class 0, Class I and Flat spectrum sources (from 28 to 20 AU; Tobin et al. in prep.), contrary to expectations from viscous disk evolution, which may be an indication of dust radial drift. The distribution of disk radii from the hydrodynamical simulation by Bate (2018) is similar to that observed for Class 0 objects, indicating that the effect of magnetic braking may not be as large as previously suggested.

In addition to these new continuum surveys, ALMA has established Keplerian rotation in four Class 0 disks (Murillo et al. 2013; Lindberg et al. 2014; Codella et al. 2014; Yen et al. 2017). A Keplerian disk was also discovered around a likely Class 0

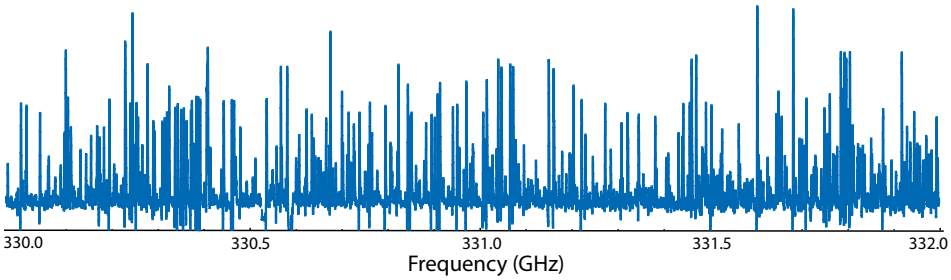

Figure 1.9: A small part of the ALMA spectrum (total spectral range of 33.7 GHz) toward the Class 0 protostar IRAS 16293B observed in the Protostellar Interferometric Line Survey (PILS; Jørgensen et al. 2016), illustrating the extreme line-richness of this source (one line every ∼3.4 MHz). Each vertical line corresponds to a molecular transition; the vertical scale is 1 Jy beam^{-1}, whereas the rms is ∼10 mJy beam^{-1}.

proto-brown dwarf (Hsieh et al. 2019), as well as a disk around a triple Class 0 protostellar system (Tobin et al. 2016a). Moreover, the disk and envelope kinematics have been studied in more detail for the Class 0 source L1527 IRS, and for several Class I sources (e.g., Yen et al. 2014; Aso et al. 2017). Other exciting results include evidence for a disk wind and grain growth in a Class I disk (Bjerkeli et al. 2016b; Harsono et al. 2018), and a possible misalignment between the inner (<40–60 AU) and outer disk of L1527 (Sakai et al. 2019).

ALMA also allows for chemical studies on disk-scales. The first of such studies have focussed on the interface between the disk and the envelope, where a possible accretion shock could cause some of the icy grain mantles to sublimate. A change in chemical composition at the disk-envelope interface has been observed for several protostars, although which molecules trace certain spatial scales differs from source to source (Sakai et al. 2014b; Oya et al. 2016). A detailed chemical study has been performed for the the low-mass protostellar binary IRAS 16293. This sources was already known to be chemically rich, but the Protostellar Interferometric Line Survey performed with ALMA (PILS) has started to reveal the full chemical complexity down to 50-AU scales (**Fig. 1.9**, e.g., Jørgensen et al. 2016). A first chemical survey toward 12 Class I sources in ρ Ophiuchus, some of which have a Keplerian disk, has recently been presented by Artur de la Villarmois et al. (2019). For these systems, $C^{17}O$ is detected towards the less evolved and less luminous sources, while SO_2 is detected toward the most evolved sources with a high luminosity. Surprisingly, no methanol is detected, suggesting that maybe only a small portion of the disks have temperatures above ∼100 K. In contrast, several complex molecules (CH_3OH, CH_2DOH, CH_3SH, NH_2CHO) have been observed toward the Class 0 source HH212-MM1, but whether their emission originates from the disk surface, a disk wind or an accretion shock at the disk-envelope interface is not yet constrained (Lee et al. 2017; Bianchi et al. 2017).

1.4.4 Modeling of embedded-disk temperature and composition

Temperature is an important parameter in disk evolution and planet formation. It governs, for example, how resistive the gas is to gravitational instabilities (e.g., Offner et al. 2010). Such instabillities could form stellar companions (e.g., Tobin et al. 2016a) and giant planets (e.g., Boss 1997; Boley 2009), or cause luminosity outbursts (e.g.,

Vorobyov 2009). In addition, temperature has a strong effect on the chemical composition of the disk through freeze-out of the major carbon and oxygen carrying species. Models for disks without an envelope have shown that higher mass accretion rates result in warmer disks (e.g., Min et al. 2011). Since accretion rates are expected to be higher during earlier stages, embedded disks may be warmer than evolved protoplanetary disks. The temperature is further influenced by the envelope which acts as an insulating blanket (e.g., D'Alessio et al. 1997; Whitney et al. 2003). In particular, Harsono et al. (2015) showed that the H_2O, CO_2 and CO snowlines are shifted to larger radii in strongly accreting young embedded disk compared to protoplanetary disks. CO is even expected to be largely present in the gas phase in embedded disks.

The absence of CO ice in embedded disks would mean that the chemical composition of the disk is not fully inherited from the molecular cloud core, where most CO is frozen out. Whether the disk material is inherited from the parental cloud, or whether it is processed, or even completely reset to atoms, on the way to the disk, is still an open question. Physicochemical models of disk formation by Visser et al. (2009b) and Visser et al. (2011) have shown that not all ices are directly incorporated into the disk. Volatile species can have desorbed and even recondensed along the way. These models do not take accretion heating into account, which could mean that ice reprocessing may occur in a larger region of the disk. In addition, Drozdovskaya et al. (2016) show that processing of ices during infall can lead to enhancement of CO_2 ice and organics at the expense of CO and methanol ice, respectively.

1.5 This thesis

ALMA has firmly established the presence of rotationally supported disks during the embedded stage of star formation. Although it remains an open question whether most young disks are large or small, and thus what the exact formation mechanism is, it is not impossible to form large $R \gtrsim$50–100 AU disks already in the Class 0 phase. Moreover, there is more and more evidence that the first steps of planet formation already occur in these young disks, instead of in more evolved protoplanetary disks, as was generally assumed. Embedded disks thus provide the true initial conditions for planet formation. Therefore, in order to understand how planets form and what composition they have, we have to know the physical and chemical conditions during this crucial early phase. Such studies are now possible with ALMA. This thesis focusses mainly on the temperature structure of embedded disks, since this is an important parameter for disk evolution and composition, and the consequences for the chemistry. The following questions are addressed:

- Are young embedded disks cold ($T \lesssim$20–25 K), such that there is a large region where CO is frozen out as observed for protoplanetary disks, or too warm for CO ice ($T \gtrsim$20–25 K), as predicted by models?

- Is the temperature profile in young disk-like structures that are not rotationally supported similar to that of embedded Keplerian disks? What are the effects on the chemistry?

- Do disks have a large reservoir of complex organic molecules? And if so, does the chemical composition resembles that of younger protostellar systems?

The first part of the thesis focusses on the temperature regime of CO freeze-out ($\lesssim$20–25 K) and investigates how robust N_2H^+ is as a tracer of the CO snowline. Moreover, the question of how to disentangle disk and envelope emission is addressed. The temperature structure is then examined in the edge-on young disks L1527 using N_2D^+, ^{13}CO and $C^{18}O$ observations, and in a larger sample of young disks using observations of $C^{17}O$ and H_2CO. The second part of the thesis concentrates on temperatures at which water and complex organics are present in the gas phase ($\gtrsim$100–150 K). First, $H^{13}CO^+$ is demonstrated to be a tracer of the water snowline. Second, the location of the water snowline and the complex molecular reservoir are studied in the young disk around the outbursting star V883 Ori. Finally, multiple H_2CS lines are used to derive the temperature profile of the disk-like structure in the Class 0 protostar IRAS 16293A.

1.5.1 Overview of chapters

The $\lesssim$ 20-25 K regime: freeze-out of CO

CHAPTER 2 - Robustness of N_2H^+ as tracer of the CO snowline
N_2H^+ has often been used to trace CO freeze-out in dense cores and protoplanetary disks. This Chapter presents a simple network containing the reactions essential for N_2H^+ chemistry, applies this to a physical model for the TW Hya protoplanetary disk and studies the correlation between N_2H^+ emission and the CO snowline. The main conclusion is that the N_2H^+ emission peaks at larger radii than the snowline, as far as $\sim$50 AU further out. This is because the 50% reduction in gaseous CO at the snowline is not yet enough to diminish N_2H^+ destruction, and because N_2H^+ can form in a surface layer where CO is already photodissociated while N_2 is not. These models place the CO snowline at 19 AU in TW Hya, $\sim$10 AU closer in than previously derived from N_2H^+ observations without taking the chemistry into account, but in agreement with $^{13}C^{18}O$ observations. Simple chemical modeling and a source-specific physical model are thus required to derive the CO snowline location from N_2H^+ observations.

CHAPTER 3 - Unveiling the physical conditions of the youngest disk: A warm embedded disk in L1527
Prompted by the non-detection of N_2D^+ in archival ALMA observations toward L1527, this Chapter aims to determine whether the young disk is indeed warm enough to prevent CO freeze-out. Since this disk is viewed edge-on, CO freeze-out is expected to be directly observable in the ^{13}CO and $C^{18}O$ observations. This Chapter shows first how disk emission can be disentangled from the envelope contribution based on kinematics and line optical depth effects. A power law radial temperature profile constructed from the brightness temperature of the optically thick ^{13}CO and $C^{18}O$ emission shows that the temperature is above 20 K out to at least 75 AU, and possibly throughout the entire 125 AU disk. Radiative transfer modeling for a L1527-specific physical structure shows that a model without CO freeze-out matches the $C^{18}O$ observations better than a model with the CO snowline at $\sim$70 AU. The young disk around L1527 is thus likely to be too warm for CO freeze-out, in contrast to more mature protoplanetary disks.

CHAPTER 4 - Temperature structure of embedded disks: Young disks in Taurus are warm
To address the question whether young embedded disks are generally warmer than protoplanetary disks, this Chapter presents ALMA observations of $C^{17}O$ and H_2CO toward five young disks in Taurus. Signs of CO freeze-out are only observed in the large disk around the borderline Class I – Class II source IRAS 04302 (at radii $\gtrsim$100 AU). In addition, H_2CO emission in IRAS 04302 originates from the surface layers. These results suggest that the midplane temperature is $\gtrsim$ 20 K but $\lesssim$ 50 K, such that H_2CO is frozen out while CO can remain in the gas phase. Young embedded disks thus seem indeed to be warmer than their more evolved counterparts.

The $\gtrsim$ 100-150 K regime: thermal desorption of H_2O and COMs

CHAPTER 5 - Imaging the water snowline in protostellar envelopes with $H^{13}CO^+$: The case of NGC1333 IRAS2A
This Chapter investigates whether $H^{13}CO^+$ can be used as a tracer of the water snowline. Although, ultimately, one wants to locate the water snowline in disks directly, protostellar envelopes are better targets to test the HCO^+-H_2O anticorrelation. First, the snowline is located at radii of 10s–100 AU instead of a few AU due to the higher accretion rates and lower densities in envelopes as compared to disks. Second, $H_2^{18}O$ has been observed in four protostellar systems, while no warm water images exist for disks. A spatial anticorrelation between $H^{13}CO^+$ and $H_2^{18}O$ emission is indeed observed with NOEMA toward the Class 0 source NGC1333 IRAS2A. Chemical and radiative transfer modeling shows that the $H^{13}CO^+$ abundance should decrease by at least a factor of six to match the observations and that this abundance drop occurs just outside the water snowline (as was shown for N_2H^+ and the CO snowline in Chapter 2). These results thus provide proof of concept that $H^{13}CO^+$ can be used as a tracer of the water snowline.

CHAPTER 6 - Imaging the water snowline in protostellar envelopes with $H^{13}CO^+$: A small survey of protostars in Perseus
This Chapter establishes $H^{13}CO^+$ as a tracer of the water snowline by observing $H^{13}CO^+$ and COMs toward four Class 0 protostars in Perseus. B1-c provides a textbook example of $H^{13}CO^+$ emission surrounding centrally peaked emission from several COMs. In addition, the compact $H^{13}CO^+$ emission toward HH 211 is consistent with the lower luminosity of this source, or the potential presence of a disk, which would result in a snowline location too close to the star to be resolved at the 0.5″ resolution of the observations. The $H^{13}CO^+$ emission displays a more complex morphology for L1448-mm with blueshifted absorption, possibly due to the presence of a wind, and seems associated with larger scales in the overall line-poor source B5-IRS1. $H^{13}CO^+$ is thus a promising tracer of the water snowline, given that the source physical structure is taken into account.

CHAPTER 7 - Methanol and its relation to the water snowline in the disk around the young outbursting star V883 Ori
A water snowline location has been claimed for one disk, V883 Ori, based only indirectly on continuum observations. However, the relation between snowlines and structures in the dust are still debated. This Chapter presents ALMA observations of

methanol (CH_3OH), a molecule expected to be released from the ice inside the water snowline. The methanol follows the Keplerian velocity structure observed for $C^{18}O$, thus the emission originates in the disk and not the envelope or outflow. The derived outer radii of ∼120–140 AU (compared to the 360 AU outer radius for $C^{18}O$), together with a rotational temperature of ∼100 K, suggest that the water snowline can be as far out as ∼100 AU, instead of the previously inferred 42 AU. Detailed modeling with a physical structure for V883 Ori is required to confirm this. In addition, methyl formate (CH_3OCHO) and acetaldehyde (CH_3CHO) are tentatively detected. Disks around outbursting young stars are thus good sources to study the chemical complexity of the planet-forming material.

CHAPTER 8 - Temperature profiles of young disk-like structures: the case of IRAS 16293A
This Chapter uses observations of multiple H_2CS lines from the ALMA Protostellar Interferometric Line Survey (PILS) to study the temperature structure of the Class 0 protostar IRAS 16293A. This source displays rotation on scales $\lesssim$ 400 AU and the presence of a Keplerian disk has been suggested in the inner ∼50 AU. However, analysis of the same H_2CS line in this Chapter shows that the high velocities attributed to a Keplerian disk are more likely a contamination by weak lines at nearby frequencies. Temperature profiles based on line ratios and rotation diagrams for the H_2CS peak fluxes show that the temperature remains $\gtrsim$ 100 K in the inner 150 AU and drops to ∼75 K at 200 AU. This is consistent with previously derived temperature profiles assuming an envelope structure. Interestingly, the temperature does not increase above ∼100–150 K in the inner 150 AU. High-resolution observations of optically thin lines are needed to establish whether this is the result of effective cooling by water that is released from the grains or due to a putative disk. Over the entire 150 AU, the temperature is ∼100 K higher than for the L1527 disk, consistent with the higher luminosity (due to a higher accretion rate) of IRAS 16293A.

1.5.2 General conclusions and outlook

The main conclusions from this thesis can be summarized as follows (see Fig. 1.10):

- Molecules such as N_2H^+ and $H^{13}CO^+$ can be used to trace the CO and H_2O snowline, respectively, as long as chemical effects are taken into account and a source-specific physical structure is employed.
- Dust continuum structures are not necessarily related to water snowlines in embedded disks.
- Young embedded disks are warm, with temperatures too high for CO freeze-out ($T \gtrsim$ 20–25 K). This is in contrast with more evolved protoplanetary disks that have large cold outer regions where CO is frozen out.
- Envelope temperature profiles (typically, $T \propto r^{-0.7}$ in the optically thick regime) are likely adequate for disk-like structures in Class 0 sources, except in the inner most region ($\lesssim$ 100 AU) that can now be probed by ALMA.
- Young disks around outbursting stars are good sources to study the ice composition of planet-forming material through thermally desorbed complex molecules.

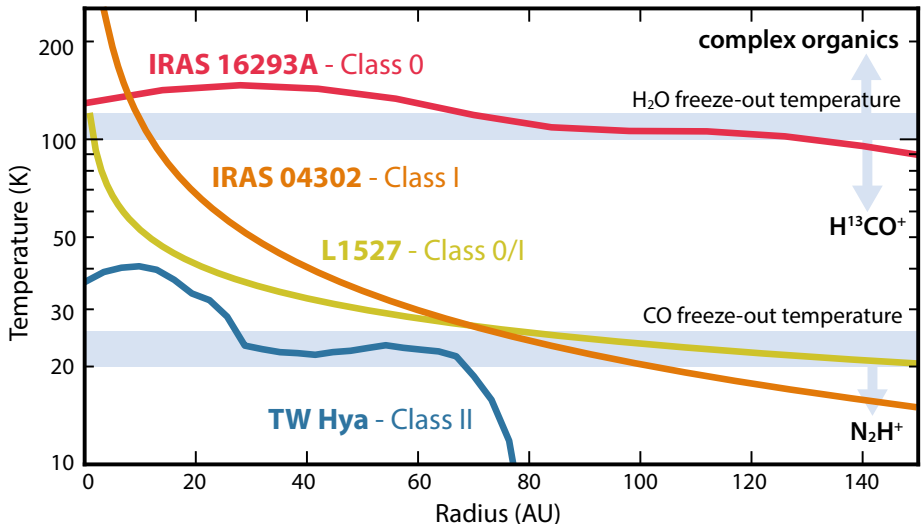

Figure 1.10: Summary of the main results in this thesis. The midplane temperature profiles for young disks show a decrease in temperature with evolution. The temperature for the disk-like structure around the Class 0 protostar IRAS 16293A (red line) is determined from H_2CS line ratios (**Chapter 8**). The midplane temperature for the Class 0/I disk L1527 (yellow line) is constructed based on opticallly thick ^{13}CO and $C^{18}O$ emission (**Chapter 3**), and $C^{17}O$ and H_2CO observations are used for the Class I disk IRAS 04302 (**Chapter 4**). These young disks are warmer than more evolved protoplanetary disks such as TW Hya (Schwarz et al. 2016). Freeze-out of CO ($T \lesssim 20-25$ K) can be traced with N_2H^+ if chemical considerations and the source physical structure are taken into account (**Chapter 2**) and $H^{13}CO^+$ is a promising tracer for the water snowline (**Chapters 5** and **6**). Complex organic molecules are released into the gas phase inside the water snowline ($T \gtrsim 100-150$ K) and can therefore be observed in young disk-like structures such as IRAS 16293A and young disks around outbursting protostars such as V883 Ori (**Chapter 7**). Although embedded disks are warm, they are not warm enough ($T \lesssim 100$ K) to have a large region where gas-phase methanol is abundant (**Chapter 4**).

This thesis provides some of the first observational constraints on the temperature structure in young disks and disk-like structures, suggesting that the temperature decreases with decreasing envelope mass and accretion rate, as expected from modeling results. Observations of more sources are now required to confirm this evolutionary trend. In addition, follow-up studies will allow more detailed questions to be answered, such as, when exactly do disks become cold enough for CO freeze-out? Already in the embedded phase, or only after the envelope has fully dissipated? What does the detailed temperature profile look like? Continuum surveys of all protostars in several star-forming regions have paved the way to answer these questions, but an important next step is to establish which sources display Keplerian rotation. Gas radii and masses of a large sample of young disks, and how they compare to values derived from continuum emission, will further our understanding of disk formation and evolution. Whether or not there is a difference in temperature structure between rotationally supported disks and disk-like structures may provide additional constraints. As shown in this thesis, the global temperature structure can be constrained with observations from simple molecules like N_2H^+ and $H^{13}CO^+$. This presents an efficient way for

an initial characterization of the large sample of disk (candidates) that can now be studied with ALMA.

Another open question is whether the composition of planet-forming material is inherited from the natal cloud, processed en route to the disk or even completely reset. On the one hand, the absence of CO freeze-out in young disks suggest that no full inheritance takes place. On the other hand, the absence of CO ice will limit the formation of COMs in the embedded disk. The presence of COMs in the V883 Ori disk therefore indicates that no complete reset takes place either. What fraction of the material gets inherited, however, remains an open question. Moreover, how much the material is altered upon entering the disk, for example, through a possible accretion shock at the disk-envelope interface, is still uncertain. Observations of young disks around outbursting protostars can shed light on this matter by providing inventories of complex species that can be compared to protostellar envelopes.

A related problem are the low abundances of CO and H_2O in protoplanetary disks. Initial results presented in this thesis show no signs of heavy CO depletion in younger disks, and future studies of embedded sources may provide clues to the evolution of planet-forming material in the disk. Another important step in our understanding of planet formation would be the direct observation of the water snowline in a disk using molecular line observations. This thesis shows that $H^{13}CO^+$ is a promising snowline tracer, and the disk around the outbursting star V883 Ori is an obvious candidate for such observations. Finally, a next step would be to incorporate the physical and chemical results for young disks into planet formation models.